Langmuir

Article

pubs.acs.org/Langmuir

# Synthesis and Self-Assembly of Perylenetetracarboxylic Diimide Derivatives with Helical Oligo(L-lactic acid)$_n$ Segments

Jun Zhou,[†] Lin Xue,[†] Yan Shi,[†] Xiyou Li,*[,†] Qingbin Xue,*[,†] and Shuangqing Wang*[,‡]

[†]Key Laboratory of Colloid and Interface Chemistry, Ministry of Education, Department of Chemistry, Shandong University, Jinan 250100, China

[‡]Key Laboratory of Photochemistry, Institute of Chemistry, Chinese Academy of Sciences, Beijing 100190, China

Supporting Information

**ABSTRACT:** Three perylenetetracarboxylic diimide (PDI) derivatives consisting of a short oligo(L-lactic acid)$_n$ (O-LLA) segment at one imide nitrogen were synthesized. The polymers were characterized by $^1$H NMR and gel permeation chromatography (GPC). Their properties were investigated by differential scanning calorimetry (DSC), X-ray diffraction (XRD) experiments, scanning electron microscopy (SEM), electronic absorption, and circular dichroism (CD) spectroscopy. The self-assembly behavior of these PDIs in molten state as well as in solvent was examined. It was found that the structure and the morphology of the self-assembly of these polymers depend on the relative length of the O-LLA segment. The PDIs with longer O-LLA chains present liquid crystal properties with an obvious phase transition from disordered phase to an ordered ($\alpha$) phase, which cannot be found for the PDIs with short O-LLA segments. The long O-LLA segments also caused a left-handed helicity for the aggregates of the PDIs from solution. This research demonstrated that one can control the order, aggregation mode, and morphology of the molecular aggregates by changing the length of the O-LLA chains. This information can be useful in the design of new organic materials that exhibit molecular aggregation.

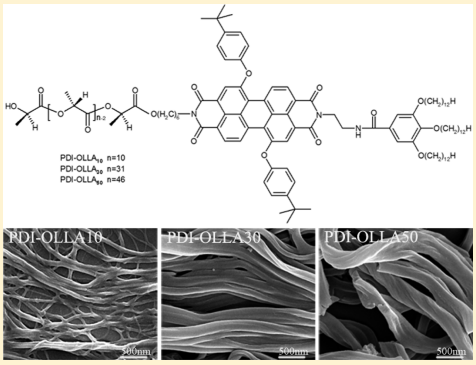


## INTRODUCTION

Perylenetetracarboxylate diimides (PDI) are currently being investigated for use in a variety of photoactive organic materials because of their low light and thermal fading rates, unique optoelectronic properties, and high luminescence efficiency.[1−3] They were widely used in light-harvesting solar cells, organic field-effect transistors, and light-emitting diodes as robust organic dyes.[4−9] They were also proved to be excellent building blocks for self-organized molecular materials with highly ordered structure due to the strong $\pi-\pi$ interactions between the planar PDI rings.[10−13]

Recently, different functional groups have been introduced to the imide nitrogen atoms or the bay (1, 2, 6, or 7) positions of PDI ring aimed at modifying the micro structures as well as the morphology of the molecular aggregates. Shinkai and co-workers have prepared a series of PDI compounds by connecting cholesterol groups at the imide nitrogen positions, which can form an organic gel with light-harvesting function.[14] Würthner and co-workers have reported a highly fluorescent organic gel based on a PDI compound functionalized with urea groups.[15] Vesicular nanocapsules prepared from amphiphilic PDI can serve as a pH sensor based on an intramolecular energy transfer mechanism.[16] Rybtchinski has prepared an amphiphilc PDI compound by connecting a long hydrophilic chain at the bay positions. This compound can form linear molecular aggregates and perform different response toward multiple outer stimuli.[17] A recyclable membrane fabricated from the self-assembly of amphiphilic PDI has also been prepared by the same group. It can be used to separate nanoparticles by size.[18] The self-assembly of PDI has also been used to fabricate a gas sensor, which shows high sensitivity toward explosives.[19,20] PDIs connected with DNA chains were prepared by Li and co-workers. The resulted thermophilic foldable polymer shows significant changes in fluorescence due to the unfolding driven by the DNA hybridization, and therefore can be used as DNA sensor.[21] Other amphiphilic diimide chromophores have also been reported recently, which can controllably self-assemble into nanotubes and might be promising functional components for mesoscopic scale opto-electronics.[22,23]

Poly(L-lactide) (PLLA) is a biodegradable semicrystalline polymer, which is widely investigated as a biomedical and biocompatible material. The mechanical properties of PLLA depend on the crystalline−amorphous structure, which vary with the crystallization conditions from the melt.[24−26] The structure of the crystals was first determined by De Santis and Kovacs[27] as left-handed $10_3$-helices (10 LLA units formed three circles) in quasi-hexagonal manner into an orthorhombic unit cell. Slight distortions of the basic helical conformation due to interchain forces were observed by vibrational spectrosco-

**Received:** January 5, 2012
**Revised:** September 6, 2012
**Published:** September 18, 2012

  

**Scheme 1. Synthesis of the Initiator PDIOH and Polymers PDI-OLLA$_n$**

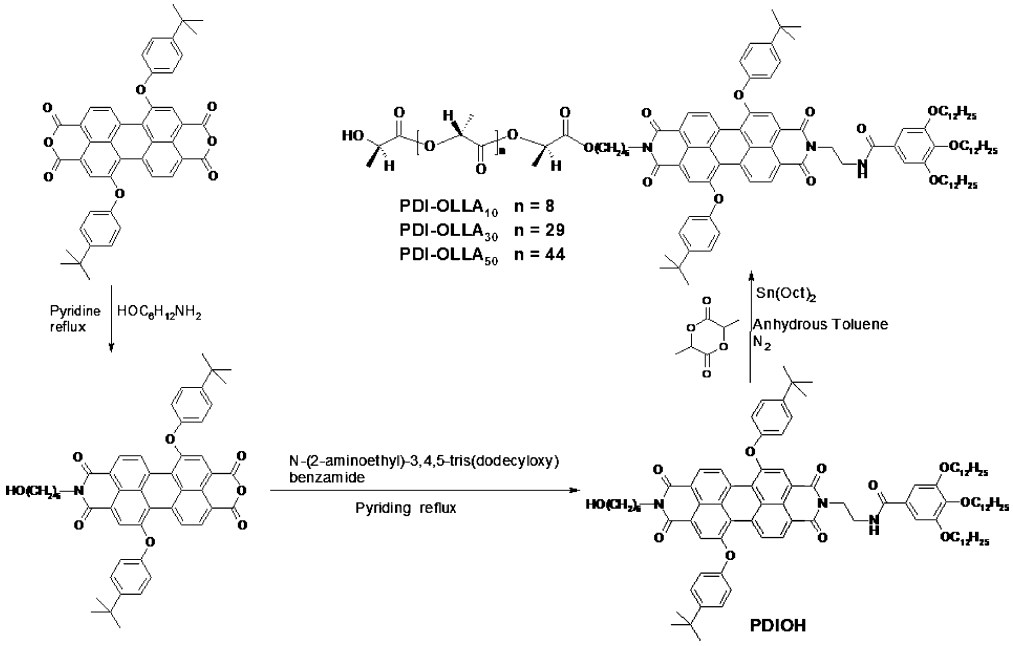


py.[28,29] Among them, helical morphologies in different length scales such as chiral centers, helical chain conformations, helical aggregations, and helical agglomerates have all been demonstrated.[30−37]

In this Article, a series of PDI-OLLA polymers with different lengths of the O-LLA segments were prepared by typical ring-opening polymerization (ROP) sequence (Scheme 1). The objective of this research is to examine the effects of liquid crystal OLLA segments on the aggregation behavior of PDI molecules, which might bring a new entry to vary the optical properties of PDIs in solid films by outer stimulus, such as temperature. On the basis of molecular weight, these polymers were labeled as PDI-OLLA$_n$, with $n$ representing the average numbers of the repeating unit for OLLA chains. The self-assembly behavior of these PDI-OLLA$_n$ polymers with different length of OLLA segments was comparatively investigated, revealing the effect of the length of the OLLA chains covalently linked to the PDI on the structure and morphology of the self-assembled nanostructures. The finding of this research will be helpful in the design of new PDI-based functional materials with controllable microstructure and morphology.

## RESULTS AND DISCUSSION

**ROP of L-LA.** Stannous octoate, SnOct2, was redistilled three times, and L-lactide (L-LA) was purified by two times recrystallization from ethyl acetate and one more time recrystallization from toluene and vacuum-dried to constant weight to remove any possible impurities containing OH groups. The ROP reaction usually is completed in 10 h at 100 °C in toluene. The synthetic procedures are shown in Scheme 1.

**Molecular Weight of PDI-OLLA$_n$.** The molecular weights of PDI-OLLA$_n$ were determined by $^1$H NMR and GPC methods. The results are summarized in Table 1. The measured molecular weights by $^1$H NMR and GPC methods were in good agreement with the theoretical prediction and found to be well controlled by the feed molar ratios of L-LA to PDIOH (Table 1).

**Table 1. Molecular Weight and Degree of Polymerization of PDI-OLLA$_n$ Obtained by $^1$H NMR and GPC Methods**

| | theoretical | | $^1$H NMR | | GPC | | |
|---|---|---|---|---|---|---|---|
| | $n$ | $M_n$ | $n$ | $M_n$ | $M_n$ | $M_w$ | $M_w/M_n$ |
| PDI-OLLA$_{10}$ | 10 | 2206 | 10 | 2206 | 1938 | 2532 | 1.31 |
| PDI-OLLA$_{30}$ | 30 | 3646 | 31 | 3722 | 3122 | 4500 | 1.44 |
| PDI-OLLA$_{50}$ | 50 | 5086 | 46 | 4798 | 4550 | 6201 | 1.36 |

**Thermal Behavior of PDI-OLLA$_n$.** The thermal behavior of these polymers was evaluated by DSC measurements. Two heat scans were performed for each sample, and the results are listed in Table 2 and Figure 1.

**Table 2. Phase Transitions of PDI-OLLA$_n$ Observed by DSC (°C)**

| samples | $T_g$ | $T_m$ | $T_i$ | $\Delta H_m$ (J/g)$^a$ | $\chi_c$ (%) |
|---|---|---|---|---|---|
| PDI-OLLA$_{10}$ | 36.2 | 140.0 | 157.2 | 1.7 | 6.0 |
| PDI-OLLA$_{30}$ | 48.2 | 143.7 | 159.6 | 16.6 | 27.9 |
| PDI-OLLA$_{50}$ | 52.5 | 146.9 | 160.8 | 28.4 | 53.0 |

$^a$The $\Delta H_m$ of the complete crystal of PLLA is 93.7 J/g.

In the first scan, PDI-OLLA$_{10}$ and PDI-OLLA$_{30}$ present three endothermic transitions, which correspond to structural relaxation associated with glass transition temperature at lower temperature range, and one transition corresponds to the melting behavior of PDI segment. Besides the three transitions observed for PDI-OLLA$_{10}$ and PDI-OLLA$_{30}$ in the low temperature range, PDI-OLLA$_{50}$ presents one more endothermic transition at about 149 °C, which corresponds to the melting behavior of the crystallized OLLA segment. In the second scan, the melting of this crystallized OLLA is not observed, as the system had a short time to undergo structural relaxation and crystallization during the cooling course after the first scan. The endothermic transition at about 159 °C can be assigned to the melting behavior of PDI segments. The $T_g$ values are more evident for the second scan than for the first


dx.doi.org/10.1021/la303061r | Langmuir 2012, 28, 14386−14394

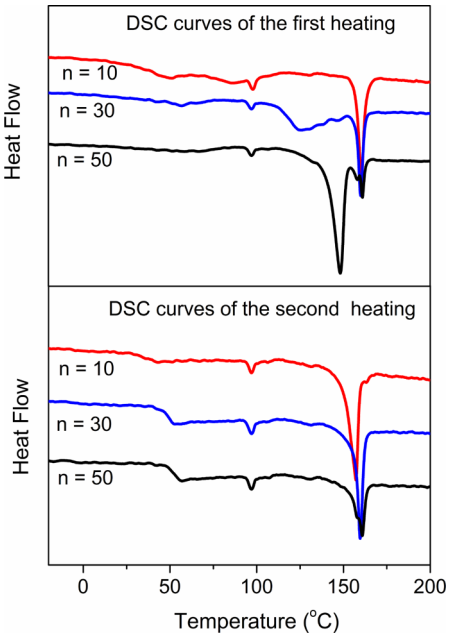


**Figure 1.** DSC scans of PDI-OLLA$_n$.

one as indicated by the increase in heat capacity reflected by the step of the traces.

Additionally, the crystallinity of the samples can be estimated on the basis of the melting enthalpy via the following equation:

$$\chi = \frac{\Delta H_m}{\Delta H_m^0 \cdot w} \times 100\%$$

where $\Delta H_m$ is the melting enthalpy of the sample, $\Delta H_m^0$ is the melting enthalpy of 100% crystalline OLLA (93.7 J/g),[38] and $w$ is the weight fraction of OLLA in the polymers. Apparently the $\chi_c$[39] values increased with the increase of OLLA chain length, indicating a stronger crystallization tendency for higher molecular weight OLLA.

**Absorption Spectra, Circular Dichroism Spectra, and Fluorescence Spectra.** UV−vis absorption and fluorescence spectra of PDIs are sensitive to the interchromophore orientation and distance[40,41] and have been widely used to study their $\pi-\pi$ stacking.[42−44] The absorption and fluorescent spectra of these compounds in chloroform are similar, and those of PDI-OLLA$_{10}$ are shown in Figure 2 as a representative. The absorption spectra of these four compounds in chloroform exhibit typical spectroscopic features that are expected for monomeric diphenoxy-substituted PDI chromophores.[13,45] The spectra show two peaks at 550 and 515 nm, which correspond to the 0−0 and 0−1 transitions, respectively.[46] The emission spectrum presents a maximum emission peak at 585 nm, which is similar to that of monomeric PDI and suggests that the PDI molecules in chloroform do not show any interactions between each other in diluted solution. Yet these polymers show significant aggregation in mixed solvents of $CHCl_3/CH_3OH$ as indicated by the blue-shifted absorption maximum and broadened absorption band (Supporting Information, Figures S1−S8).

The absorption and emission spectra of these polymers are also measured in their molten thin solid films or precipitated aggregates from solution. The thin solid films are prepared by depositing the polymer solids on a glass substrate, and then the glass substrate was heated on a hot plate to melt the sample.

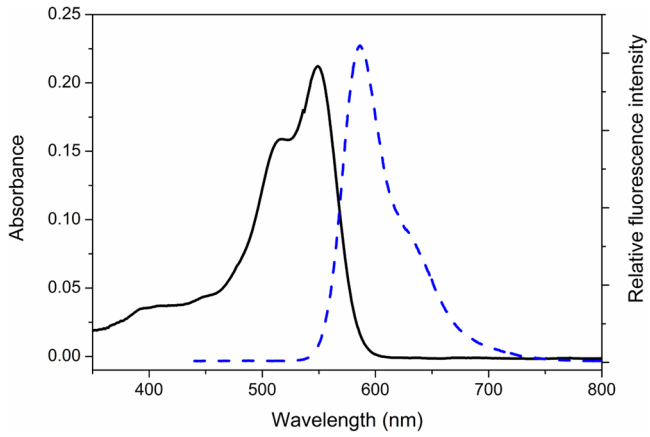


**Figure 2.** Absorption (−) and fluorescence (− − −) spectra (excited at 430 nm) of PDI-LLA$_{10}$ in chloroform ($5 \times 10^{-6}$ mol $L^{-1}$).

The molten sample (at 230 °C) was cooled to room temperature with a controlled speed (2 °C/min). The films prepared in this way were designed as molten film. The solution-precipitated aggregates were prepared by injecting a polymer solution (2 mg/mL, 1 mL) in dichloromethane into a large volume of methanol (100 mL). The resulted mixture was aged at room temperature overnight, and then the suspension of the molecular aggregates was transferred to the glass substrate by a dropper. After the solvents were evaporated to dryness at room temperature, the samples were subjected to spectroscopic and morphology examination. The solids prepared in this way are designed as aggregates. The absorption spectrum of PDI normally shows three pronounced peaks in the range of 350−575 nm, which correspond to the 0−0, 0−1, and 0−2 vibronic transitions, respectively. Yet the absorption spectra of the molten films and the aggregates of these three compounds changed dramatically from their monomer, Figure 3A and B. The transitions from ground state to the higher levels of vibration states (0−1 and 0−2) are enhanced as compared to the 0−0 transition. Such a spectral change implies strong molecular stacking between the PDI skeletons in the solid-state molten films and aggregates. Meanwhile, the pronounced absorption band at longer wavelength (575 nm) is also a typical indication of the effective $\pi-\pi$ interactions in cofacially arranged molecular stack.[47] The polarized absorption spectra of these polymers in molten film are recorded under both parallel or vertical polarized incident light. The spectra are shown in Figures S9−12 in the Supporting Information. The small difference between the absorption spectra of different polarized light suggests that the PDI units in the molten film do not pack with long-range order in one direction. This point is also supported by the SEM images as shown later.

The fluorescence spectra of the molten films of these three polymers show a broad emission band at about 670 nm, Figure 4A. The fluorescence lifetime measurement revealed longer fluorescence lifetimes for this emission band, Table 3. This band can be assigned to the emission of excimer.[13] Small differences were identified between the emission spectra of these three polymers. The maximum emission peak of PDI-OH molten film is found at 678 nm, but this peak blue-shifted to 668 nm for PDI-OLLA$_{10}$ molten film, 665 nm for PDI-OLLA$_{30}$ molten film, and 659 nm for PDI-OLLA$_{50}$ molten film. This change in the maximum emission peak can be ascribed to the influence of OLLA on the micro stacking manner of PDI units.


dx.doi.org/10.1021/la303061r | *Langmuir* 2012, 28, 14386−14394

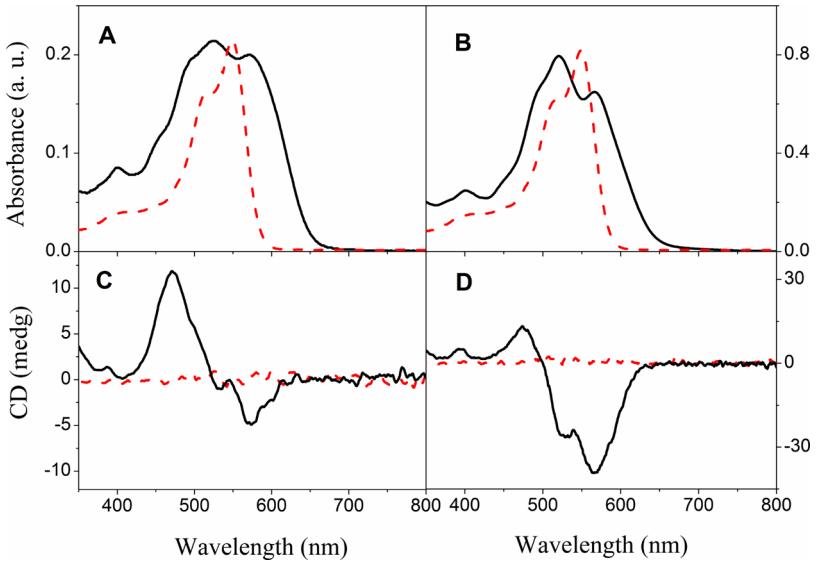


**Figure 3.** Absorption (A,B) and circular dichroism spectra (C,D) spectra of PDI-OLLA$_{10}$, in molten film (A,C) and solution precipitated aggregates films (B,D). The dashed lines are the spectra of PDIOH in solution.

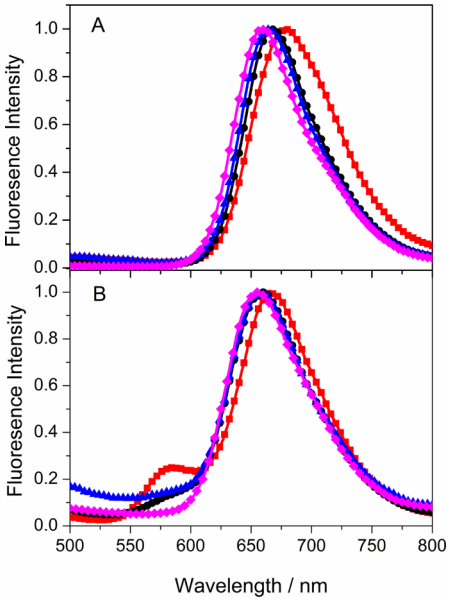


**Figure 4.** Fluorescence spectra of the molten films (A) and precipitated aggregates (B) of compounds PDIOH (■), PDI-OLLA$_{10}$ (●), PDI-OLLA$_{30}$ (▲), and PDI-OLLA$_{50}$ (◆).

**Table 3. Fluorescence Quantum Yields ($\Phi_f$) and Lifetimes ($\tau$)**

| | in chloroform | | aggregates | | molten films | |
|---|---|---|---|---|---|---|
| compounds | $\Phi_f$ | $\tau^a$ | $\Phi_f$ | $\tau^a$ | $\Phi_f$ | $\tau^a$ |
| PDIOH | 0.77 | 4.37 | 0.18 | 14.6 | 0.11 | 15.8 |
| PDI-OLLA$_{10}$ | 0.63 | 4.40 | 0.09 | 17.1 | 0.04 | 15.3 |
| PDI-OLLA$_{30}$ | 0.62 | 4.32 | 0.08 | 15.8 | 0.04 | 15.0 |
| PDI-OLLA$_{50}$ | 0.61 | 4.45 | 0.08 | 16.3 | 0.03 | 14.2 |

[a] $\tau$ values are measured at 680 nm.

A PDI dimer with rigid face-to-face stacked structure shows an excimer emission at about 705 nm,[41] but a similar dimer with relatively flexible face-to-face stacked structure shows excimer emission at about 625 nm.[48] Therefore, the blue shift of the excimer emission of these three polymers in relation to that of PDIOH might be ascribed to the deviation of the stacked structure of PDI units from a strictly face-to-face stacking to a slipped face-to-face stacking. The larger OLLA group will cause larger blue shift of the emission peak and more significant deviation from strictly face-to-face stacked structure. This means the aggregation of these polymers in molten films is affected significantly by the OLLA chains.

The fluorescence spectra of the aggregates of these three polymers are shown in Figure 4. A small emission band at about 580 nm, which can be assigned to the emission from monomeric PDI, is found for PDIOH, PDI-OLLA$_{10}$, and PDI-OLLA$_{30}$. The maximum emission bands at about 660 nm of these three polymers are similar and can be assigned to the emission of excimer based on the maximum emission wavelength and the lifetime measured.[13] This emission band show a small blue shift in comparison with that of PDIOH. This result suggests that the micro structure of the stacked PDIs in the precipitated aggregates is less sensitive to the length of the OLLA chain than that in the molten films. In another word, the aggregation process of these molecules during the precipitation from solution is probably dominated by the PDI parts of the molecules instead of the OLLA chains. More interestingly, the maximum emission band of the aggregates precipitated from solution of PDIOH is significantly blue-shifted relative to that of molten films. This means that the PDI units of PDIOH in the solution-precipitated aggregates do not form a strictly face-to-face stacked structure, but a slipped or twisted stacked structure instead. Similarly, the emission bands of these three polymers blue-shifted a little bit in relation to that of molten films. This indicates also that the PDI in the aggregates adapted a more slipped or twisted stacked structure than that in molten films.

The fluorescence quantum yields for PDIOH, PDI-OLLA$_{10}$, PDI-OLLA$_{30}$, and PDI-OLLA$_{50}$ are measured, and the results are summarized in Table 3. It can be found that the fluorescence quantum yields ($\Phi_f$) of these compounds in solution are large, which suggest that no aggregation in solution happened. Yet in the solid states, the fluorescence quantum yields decrease significantly. This can be ascribed to the


dx.doi.org/10.1021/la303061r | *Langmuir* 2012, 28, 14386−14394

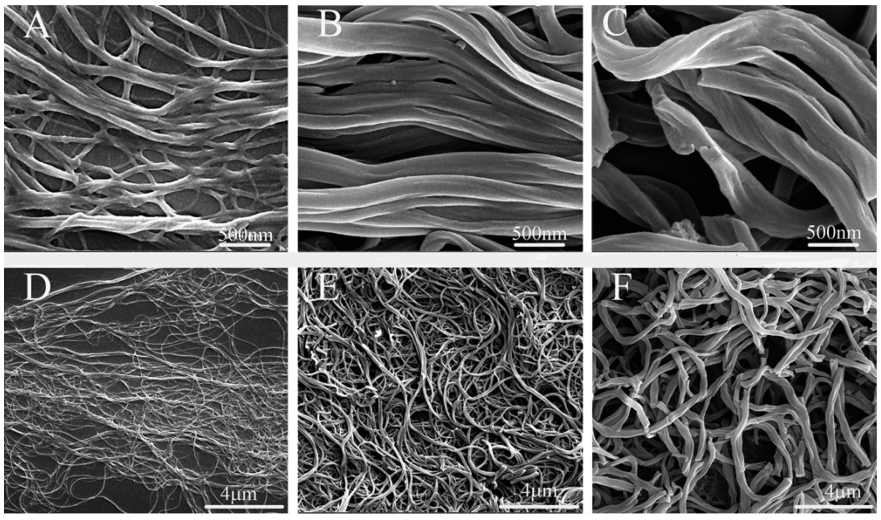


**Figure 5.** SEM images of the solution-precipitated aggregates of PDI-OLLA$_{10}$ (A,D), PDI-OLLA$_{30}$ (B,E), and PDI-OLLA$_{50}$ (C,F).

formation of H-type molecular aggregates. More importantly, the fluorescence quantum yields for the aggregates precipitated from solution show relatively larger $\Phi_f$ than that of molten films. This indicates that the stacking structure for the PDI units in the solution precipitated aggregates is more seriously slipped or twisted from the face-to-face stacking, which corresponds very well with the results of fluorescence spectra as shown in Figure 4.

In the CD spectra of the aggregates, Figure 3C and D, negative bisignate Cotton effects [570(−)/476(+)] are observed in the absorption region of PDI units for all three polymers in molten films as well as in precipitated aggregates, which indicates the presence of left-handed chirality of the dipole moment (negative chirality)[49] in the solid state. However, we do not find any CD signals in dilute chloroform solutions. According to Meskers and Aida,[50] the CD signals can be induced by the linear alignment of molecules in thin solid film. To find out the origin of these CD signals of these polymer thin solid films, we measured the CD spectra of stacked two-layer polymer films with different rotated angles of one layer against the other one following the method described by Meskers. Bisignate CD effects are observed, whose intensity depends on the angle of rotation of one layer film against the other, but the negative bisignate Cotton effects do not change (Supporting Information Figure S13). This phenomenon is similar to that observed for a chiral oligo(*p*-phenylene vinylene) compound and suggests that the CD signals obtained for the thin solid films of these three polymers are caused by both linear alignment and left-handed helical arrangement of the molecules in molten films and aggregates.[50a,51] These results confirm the effect of the long OLLA segment on tuning the PDI chromophore packing mode and supramolecular chirality in molecular aggregates. All of the compounds show similar behavior in the CD spectra; no obvious difference can be identified between these three polymers.

**Morphology of the Aggregates.** The morphologies of the precipitated aggregates are examined by scanning electron microscopy (SEM). As can be found in Figure 5, these polymers self-assemble into long, twisted fibrous nanostructures with approximately several tens of micrometers in length and hundreds of nanometers in width. Further careful inspection over these nanoribbons revealed that the dimensions of these one-dimensional nanostructures were changed along with the change in the length of OLLA chains. Longer OLLA caused the formation of short nanoribbons with large width, whereas short OLLA segments induce the formation of long fibers with small width. It is clear that these ribbons consist of bundles of single, twisted strands. The morphology of the molten films shows a flat surface; no fine structure or veins can be identified from the SEM images.

**X-ray Diffraction Patterns of the Aggregates.** To obtain information about the internal structure of the thin solid films and the aggregates precipitated from solution, XRD experiments are performed on these solids. The XRD patterns are compared in Figure 6. In the wide-angle region of the X-ray diffraction patterns obtained for the molten films, a broad peak in the region of 15−30°, with *d* space around 0.40 nm, can be found, which can be attributed to the liquid-like order of the alkyl chains.[52] In the diffraction pattern of PDI-OLLA$_{10}$, a broad diffraction peak appeared at $2\theta$ = 19.06°, which can be ascribed to the formation of PLLA crystals with small crystallite size.[53] This peak becomes more apparent for PDI-OLLA$_{30}$ and PDI-OLLA$_{50}$ molten films. A group of sharp diffraction peaks found in the same region for PDI-OLLA$_{30}$ and PDI-OLLA$_{50}$ molten films can be assigned to the (110), (100), (203), and (205) diffractions of the $\alpha$-form crystal of PLLA as have been reported by Miyata.[39] The diffraction peak at about $2\theta$ = 5.45°, corresponding to a *d* space of about 1.60 nm, can be assigned to the length of the PDI units as shown in Figure 5. The intensity of this diffraction peak decreases obviously along with the increase in the size of OLLA segment. This result suggests that the longer OLLA$_n$ segments cut down the packing order of PDI units in the molten films.

In the diffraction profile of the precipitated aggregates, the broad diffraction peak around $2\theta$ = 21° and *d* = 0.40 nm is not found, which suggests that the packing of the long alky chains in these precipitated aggregates is orderless. Yet the diffraction peak at $2\theta$ = 28.5°, with *d* = 0.31 nm, corresponding to the distance between the PDI rings of the adjacent molecules,[54] is more significant than that for the molten films. A diffraction peak at $2\theta$ = 16.4° with *d* = 0.54 nm is observed in the diffraction pattern of the precipitated aggregates of PDI-OLLA$_{50}$, which is missing in the diffraction of PDI-OLLA$_{10}$ and PDI-OLLA$_{31}$ and can be attributed to the $\alpha$-form crystal of PLLA as reported by Miyata.[39]


dx.doi.org/10.1021/la303061r | *Langmuir* 2012, 28, 14386−14394

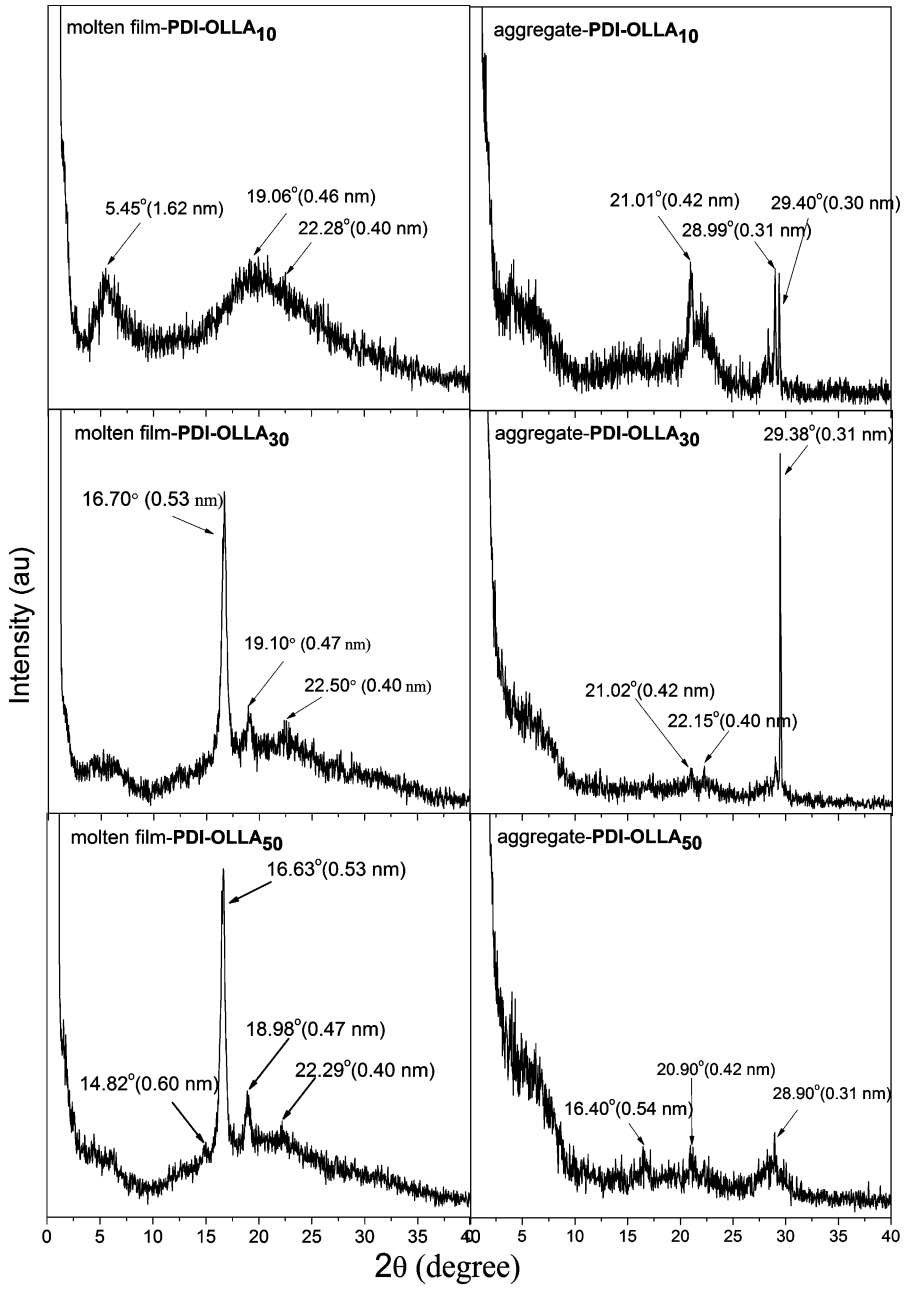


**Figure 6.** XRD scans of PDI-OLLA$_{10}$, PDI-OLLA$_{30}$, and PDI-OLLA$_{50}$.

By comparing the XRD profile of the precipitated aggregates with that of the molten thin solid film, we can conclude that the PDI aromatic rings in solution-precipitated aggregate packed with high order. However, during the cooling process from a molten state to a solid state, the aggregation of the polymer molecules is dominated by the long alkyl chains and the OLLA segment and results in a highly ordered alkyl chain packing and OLLA packing in the thin solid film. This phenomenon might be caused by the ordered alignment of OLLA segment in molten state, which drives the PDI units to change their packing structure accordingly. This results corresponding well with the results of absorption and fluorescence spectra as mentioned above.

## CONCLUSION

A series of PDI compound connected with L-lactic acid oligimers of different length have been prepared successfully. The attachment of low molecular weight L-lactic acid oligomers can significantly affect the self-assembly properties of PDI. The helicity of the L-lactic acid segments induces left-hand arrangement of the PDI units in the molten films or solution-precipitated aggregates. During the cooling process from molten state to solid state, the OLLA segment as well the long alkyl chains packed together with long-range order and had larger effects on the aggregation of PDI units and affect the fluorescence spectra significantly. However, during the precipitating from solution, both the alkyl chains and the OLLA chains do not form ordered structure. The aggregation behavior can be schematically described by Figure 7. The present results reveal that introducing liquid crystal OLLA


dx.doi.org/10.1021/la303061r | *Langmuir* 2012, 28, 14386−14394

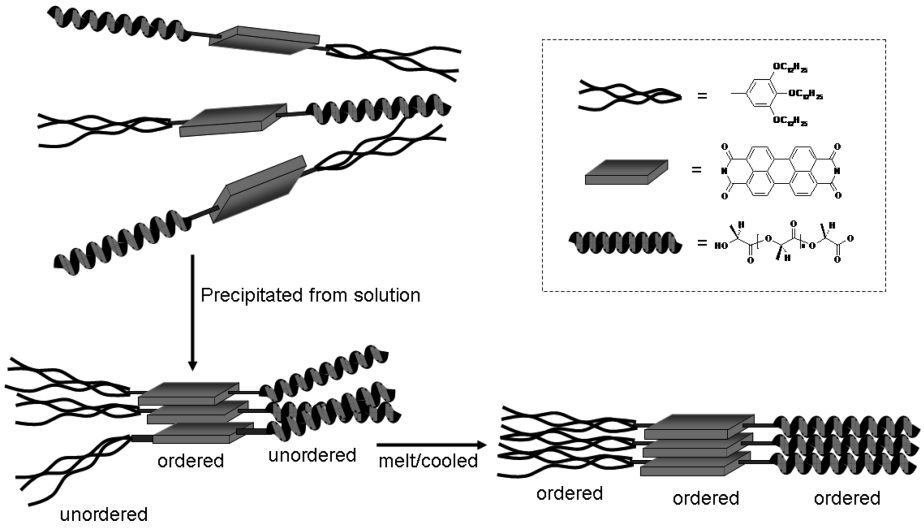


**Figure 7.** Comparison of the aggregation behavior of these polymers in solution-precipitated aggregates or molten films.

segment to a PDI derivative could introduce a special aggregation behavior for the PDI units during the solidification from a molten state. This finding might be useful for the design of novel thermal-sensitive fluorescent PDI compounds.

## EXPERIMENTAL SECTION

**Measurements and Characterization.** $^1$H NMR spectra were recorded on a Bruker DPX 300 spectrometer (300 MHz) in $CDCl_3$. Spectra were referenced internally by using the residual solvent resonance ($\delta$ = 7.26 for $CDCl_3$) relative to $SiMe_4$. GPC measurements were performed on an HPLC equipped with 515HPLC pump and HR3/HR4/HR6 columns at 1.00 mL/min using THF as eluent under 40.0 °C with polystyrene as standard (Shodex Standard SL-105, Japan). Differential scanning calorimeter (DSC) measurements were performed on a DSC-SP (Rheometric Scientific Inc., NJ) from −50−200 °C under inert $N_2$ atmosphere with a scanning rate of 10 °C/min. Typically, samples weighting about 5.0 mg were heated (10 °C/min) in Al crucibles from −50 to 200 °C. Normally two circles of heating at same scan rate were performed. Low-angle X-ray diffraction (XRD) measurements were carried out on a Rigaku D/max-$\gamma$B X-ray diffractometer with a Cu K$\alpha$ sealed tube ($\lambda$ = 0.15406 nm) at 293 K. Scanning electronic microscopy (SEM) images were obtained using a JEOL JSM-6700F field-emission scanning electron microscopy. For SEM imaging, Au (1−2 nm) was sputtered onto the grids to prevent charging effects and to improve image clarity. UV−vis absorption spectra were recorded on a Hitachi 4100 spectrometer. Fluorescence spectra and fluorescence lifetimes were recorded on a K2 system of ISS. The absolute fluorescence quantum yields of these compounds in solution as well as in films or solid aggregates were measured on a Hamamatsu Quantaurus QY instrument. Circular dichroism (CD) spectra were recorded on a J-810-150 L spectropolarimeter (Jasco, Japan).

**Materials.** L-Lactide (LLA) was purified by repeat recrystallization from ethyl acetate and toluene, respectively, and then with vacuum-drying at room temperature to constant weight. Stannous octoate, SnOct2, was redistilled three times as reported in ref 55. Toluene (AR) was refluxed over Na for 24 h, and then distilled under nitrogen atmosphere just before use. 1,7-Di(*p*-t-butyl-phenoxyl)-3,4,9,10-tetracarboxylic dianhydride[56] and *N*-(2-aminoethyl)-3,4,5-tris-(dodecyloxy) benzamide[57] were synthesized following the previously reported methods. All other chemicals were purchased from commercial source. Column chromatography was carried out on silica gel (Merck, Kieselgel 60, 70−230 mesh) with the indicated eluent. All other reagents and solvents were used as received without further purification.

*N-Amino-1-hexanol-1,7-di(p-t-butyl)phenoxy-perylene-3,4-dicarboxylic anhydride- 9,10-dicarboxyimide.* 1,7-Di(*p*-*t*-butyl-phenoxyl)-3,4,9,10-tetracarboxylic dianhydride (500 mg, 0.73 mmol) was dissolved in 30 mL of pyridine, and a solution of 6-amino-1-hexanol (85 mg, 0.73 mmol) in 20 mL of pyridine was added dropwise. The mixture was refluxed at 116 °C for 1.5 h. After being cooled to room temperature, the solvent was evaporated. The residue was purified by column chromatography on silica gel ($CH_2Cl_2$ as eluent) (57.4 mg, 10%). $^1$H NMR (300 MHz, $CDCl_3$): $\delta$ = 9.65 (m, 2H), 8.65 (m, 2H), 8.35 (d, 2H), 7.50−7.53 (d, 4H), 7.13 (d, 4H), 4.15 (t, 2H), 3.63 (t, 2H), 1.25−1.71 (m, 26H). MS (MALDI-TOF): *m*/*z*, calculated for $C_{50}H_{45}NO_8$, 787.32; found, 787.90 [$M^+$].

*N-Amino-1-hexanol-N′-(2-aminoethyl)-3,4,5-tris(dodecyloxy) Benzamide-1,7-di(p-t-butylphenoxy)perylene-3,4;9,10-tetracarboxylate Diimide.* A mixture of *N*-amino-1-hexanol-1,7-di(*p*-*t*-butyl)-phenoxy-perylene-3,4-dicarboxylic anhydride-9,10-dicarboxyimide (200 mg, 0.254 mmol), *N*-(2-aminoethyl)-3,4,5-tris(dodecyloxy) benzamide (500 mg, 0.70 mmol), and pyridine (15 mL) was heated to 116 °C under $N_2$ atmosphere. The reaction mixture was stirred continuously for 60 min at this temperature until the reaction finished from the detection of TLC. The solvent was evaporated under reduced pressure, and the residue was purified by column chromatography on silica gel with chloroform as eluent. The main fraction contains product HOPDI (302.2 mg, yield 80%). MALDI-TOF MS (*m*/*z*): calcd for $C_{95}H_{127}N_3O_{11}$, 1485.95; found, 1487.03. $^1$H NMR (CDCl3, 300 MHz): $\delta$ 9.57−9.53 (m, 2H), 8.65−8.62 (m, 2H), 8.29 (s, 1H), 8.26 (s, 1H), 7.47 (d, 4H), 7.09 (d, 4H), 6.9 (d, 2H), 4.55 (t, 2H), 4.12 (t, 2H), 3.99−3.84 (b, 8H), 3.60 (b, 2H), 1.83−1.66 (b, 6H), 1.59 (m, 2H), 1.25−1.22 (m, 54H), 0.88 (t, 9H).

**Ring-Opening Polymerization of L-LA.** A general procedure for the ring-opening polymerization (ROP) of L-LA was shown in Scheme 1. The feed ratios of LLA to HOPDI and SnOct2 were adjusted to get oligomers/polymers of different molecular weight. The procedure was briefly described as follows:[58] the proper amount of L-LA, HOPDI were vacuum-dried at near 50 °C for 3 h and then mixed with $SnOct_2$ solution in toluene with a typical ratio (*x*:1:1, *x* = 5, 15, 25) and toluene. After being stirred for 10 h at 100 °C, the viscous mixture was cooled and evaporated to dry. Next, the residual was dissolved in $CH_2Cl_2$ and washed with 1 M HCl aqueous and water, respectively. After being concentrated under reduced pressure to a third of the volume, the solution was then poured into petroleum ether. The precipitate was collected as the targeted compounds.

**PDIOPLLA$_{10}$.** $^1$H NMR ($CDCl_3$, 300 MHz): $\delta$ 9.60 (q, 2H), 8.69−8.59 (m, 2H), 8.38 (d, 1H), 8.28 (s, 1H), 7.47 (d, 4H), 7.09 (d, 4H), 6.92 (d, 2H), 5.23−5.01 (m, 10H), 4.52 (d, 2H), 4.38−4.32 (m, 1H), 4.11 (m, 2H), 3.99−3.92 (b, 6H), 3.60 (b, 2H), 1.78−1.68 (m, 6H), 1.37 (s, 9H), 1.25−1.22 (m, 54H), 0.87(t, 9H).


dx.doi.org/10.1021/la303061r | *Langmuir* 2012, 28, 14386−14394

**PDIOPLLA$_{30}$.** $^1$H NMR ($CDCl_3$, 300 MHz): $\delta$ 9.66 (q, 2H), 8.69−8.58 (m, 2H), 8.38 (d, 1H), 8.28 (s, 1H), 7.47 (d, 4H), 7.09 (d, 4H), 6.92 (d, 2H), 5.25−5.10 (m, 31H), 4.56 (d, 2H), 4.38−4.32 (m, 1H), 4.14 (m, 2H), 4.02−3.92 (b, 6H), 3.60 (b, 2H), 1.78−1.68 (m, 6H), 1.37 (s, 9H), 1.25−1.23 (m, 54H), 0.87 (t, 9H).

**PDIOPLLA$_{50}$.** $^1$H NMR ($CDCl_3$, 300 MHz): $\delta$ 9.60 (q, 2H), 8.69−8.59 (m, 2H), 8.38 (d, 1H), 8.28 (s, 1H), 7.47 (d, 4H), 7.09 (d, 4H), 6.92 (d, 2H), 5.20−5.13 (m, 43H), 4.57 (d, 2H), 4.38−4.32 (m, 1H), 4.12 (m, 2H), 3.98−3.92 (m, 6H), 3.60 (m, 2H), 1.80−1.68 (m, 6H), 1.37 (m, 9H), 1.25−1.23 (m, 54H), 0.87 (t, 9H).

## ■ ASSOCIATED CONTENT

### Supporting Information

Absorption spectra of PDI-OLLA$_n$ in chloroform with different contents of methanol. Polarized absorption spectra of the solution precipitated aggregates and the molten films. CD spectra of two-layer stacked molten films at different rotation angles between the two layers. This material is available free of charge via the Internet at http://pubs.acs.org.

## ■ AUTHOR INFORMATION

### Corresponding Author

*E-mail: xiyouli@sdu.edu.cn.

### Notes

The authors declare no competing financial interest.

## ■ ACKNOWLEDGMENTS

Financial support from the Natural Science Foundation of China (21073112, 21173136) and the Natural Science Foundation of Shandong Province (ZR2010EZ007) is gratefully acknowledged.

## ■ REFERENCES

(1) Feng, J.; Liang, B.; Li, X. Synthesis and Aggregation Behavior of Perylenetetracarboxylic Diimide Trimers with Different Substituents at Bay Positions. *Langmuir* **2008**, *24*, 11209−11215.

(2) Gregg, B. A. Excitonic Solar Cells. *J. Phys. Chem. B* **2003**, *107*, 4688−4698.

(3) Cormier, R. A.; Gregg, B. A. Synthesis and Characterization of Liquid Crystalline Perylene Diimides. *Chem. Mater.* **1998**, *10*, 1309−1319.

(4) Lehn, J. M. Toward Self-Organization and Complex Matter. *Science* **2002**, *295*, 2400−2403.

(5) Tanaka, S.; Shirakawa, M.; Kaneko, K.; Takeuchi, M.; Shinkai, S. Porphyrin-Based Organogels: Control of the Aggregation Mode by a Pyridine−Carboxylic Acid Interaction. *Langmuir* **2005**, *21*, 2163−2172.

(6) Li, X.; Sinks, L. E.; Rybtchinski, B.; Wasielewski, M. R. Ultrafast Aggregate-to-Aggregate Energy Transfer within Self-assembled Light-Harvesting Columns of Zinc Phthalocyanine Tetrakis-(Perylenediimide). *J. Am. Chem. Soc.* **2004**, *126*, 10810−10811.

(7) Sinks, L. E.; Rybtchinski, B.; Iimura, M.; Jones, B. A.; Goshe, A. J.; Zuo, X.; Tiede, D. M.; Li, X.; Wasielewski, M. R. Self-Assembly of Photofunctional Cylindrical Nanostructures Based on Perylene-3,4:9,10-bis(dicarboximide). *Chem. Mater.* **2005**, *17*, 6295−6303.

(8) Wang, W.; Han, J. J.; Wang, L.-Q.; Li, L.-S.; Shaw, W. J.; Li, A. D. Q. Dynamic $\pi-\pi$ Stacked Molecular Assemblies Emit from Green to Red Colors. *Nano Lett.* **2003**, *3*, 455−458.

(9) van Gorp, J. J.; Vekemans, J. A. J. M.; Meijer, E. W. $C_3$-Symmetrical Supramolecular Architectures: Fibers and Organic Gels from Discotic Trisamides and Trisureas. *J. Am. Chem. Soc.* **2002**, *124*, 14759−14769.

(10) Dehm, V.; Chen, Z.-J.; Baumeiste, U.; Prins, P.; Siebbeles, L. D. A.; Würthner, F. Helical Growth of Semiconducting Columnar Dye Assemblies Based on Chiral Perylene Bisimides. *Org. Lett.* **2007**, *9*, 1085−1088.

(11) Yan, P.; Chowdhury, A.; Holman, M. W.; Adams, D. M. Self-Organized Perylene Diimide Nanofibers. *J. Phys. Chem. B* **2005**, *109*, 724−730.

(12) Zhang, X.; Chen, Z.; Würthner, F. Morphology Control of Fluorescent Nanoaggregates by Co-Self-Assembly of Wedge- and Dumbbell-Shaped Amphiphilic Perylene Bisimides. *J. Am. Chem. Soc.* **2007**, *129*, 4886−4887.

(13) Wang, Y.; Chen, Y.; Li, R.; Wang, S.; Su, W; Ma, P.; Wasielewski, M. R.; Li, X.; Jiang, J. Amphiphilic Perylenetretracarboxyl Diimide Dimer and Its Application in Field Effect Transistor. *Langmuir* **2007**, *23*, 5836−5842.

(14) Sugiyasu, K.; Fujita, N.; Shinkai, S. Visible-Light-Harvesting Organogel Composed of Cholesterol-Based Perylene Derivatives. *Angew. Chem., Int. Ed.* **2004**, *43*, 1229−1233.

(15) Würthner, F.; Hanke, B.; Lysetska, M.; Lambright, G.; Harms, G. S. Gelation of a Highly Fluorescent Urea-Functionalized Perylene Bisimide Dye. *Org. Lett.* **2005**, *7*, 967−970.

(16) Zhang, X.; Rehm, S.; Safont-Sempere, M. M.; Würthner, F. Vesicular Perylene Dye Nanocapsules as Supramolecular Fluorescent pH Sensor System. *Nat. Chem.* **2009**, *1*, 623−629.

(17) Krieg, E.; Shirman, E.; Weissman, H.; Shimoni, E.; Wolf, S. G.; Pinkas, I.; Rybtchinski, B. Supramolecular Gel Based on a Perylene Diimide Dye: Multiple Stimuli Responsiveness, Robustness, and Photofunction. *J. Am. Chem. Soc.* **2009**, *131*, 14365−14373.

(18) Krieg, E.; Weissman, H.; Shirman, E.; Shimoni, E.; Rybtchinski, B. Recyclable Supramolecular Membrane for Size-Selective Separation of Nanoparticles. *Nat. Nanotechnol.* **2011**, *6*, 141−146.

(19) Che, Y.; Yang, X.; Liu, G.; Yu, C.; Ji, H.; Zuo, J.; Zhao, J.; Zang, L. Ultrathin n-Type Organic Nanoribbons with High Photoconductivity and Application in Optoelectronic Vapor Sensing of Explosives. *J. Am. Chem. Soc.* **2010**, *132*, 5743−5750.

(20) Che, Y.; Yang, X.; Loser, S.; Zang, L. Expedient Vapor Probing of Organic Amines Using Fluorescent Nanofibers Fabricated from an n-Type Organic Semiconductor. *Nano Lett.* **2008**, *8*, 2219−2223.

(21) Wang, W.; Wan, W.; Zhou, H.-H.; Niu, S.; Li, A. D. Q. Alternating DNA and $\pi$-Conjugated Sequences. Thermophilic Foldable Polymers. *J. Am. Chem. Soc.* **2003**, *125*, 5248−5249.

(22) Rao, K. V.; George, S. J. Synthesis and Controllable Self-Assembly of a Novel Coronene Bisimide Amphiphile. *Org. Lett.* **2010**, *12*, 2656−2659.

(23) Shao, H.; Seifert, J.; Romano, N. C.; Gao, M.; Helmus, J. J.; Jaroniec, C. P.; Modarelli, D. A.; Parquette, J. R. Amphiphilic Self-Assembly of an n-Type Nanotube. *Angew. Chem., Int. Ed.* **2010**, *49*, 7688−7691.

(24) Huang, J.; Lisowski, M. S.; Runt, J.; Hall, E. S.; Kean, R. T.; Buehler, N.; Lin, J. S. Crystallization and Microstructure of Poly(l-lactide-co-meso-lactide) Copolymers. *Macromolecules* **1998**, *31*, 2593−2599.

(25) Baratian, S.; Hall, E. S.; Lin, J. S.; Xu, R.; Runt, J. Crystallization and Solid-State Structure of Random Polylactide Copolymers: Poly(l-lactide-co-d-lactide)s. *Macromolecules* **2001**, *34*, 4857−4864.

(26) Cho, J.; Baratian, S.; Kim, J.; Yeh, F.; Hsiao, B.; Runt, J. Crystallization and Structure Formation of Poly(L-lactide-co-meso-lactide) Random Copolymers: a Time-Resolved Wide- and Small-Angle X-ray Scattering Study. *Polymer* **2003**, *44*, 711−717.

(27) Santis, P. D.; Kovacs, A. J. Molecular Conformation of Poly (S-lactic Acid). *Biopolymers* **1968**, *6*, 299−306.

(28) Aleman, C.; Lotz, B.; Puigalli, J. Crystal Structure of the $\alpha$-Form of Poly(l-lactide). *Macromolecules* **2001**, *34*, 4795−4801.

(29) Kang, S.; Hsu, S. L.; Stidhand, H. D.; Smith, P. B.; Leugers, M. A.; Yang, X. A. Spectroscopic Analysis of Poly(lactic acid) Structure. *Macromolecules* **2001**, *34*, 4542−4548.

(30) Tachibana, T.; Kambara, H. Enantiomorphism in the Helical Aggregate of Lithium 12-Hydroxystearate. *J. Am. Chem. Soc.* **1965**, *87*, 3015−3016.

(31) (a) Cornelissen, J. J. L. M.; Fischer, M.; Sommerdijk, N. A. J. M.; Nolte, R. J. M. Helical Superstructures from Charged Poly-(styrene)-Poly(isocyanodipeptide) Block Copolymers. *Science* **1998**, *280*, 1427−1430. (b) Engelkamp, H.; Middelbeek, S.; Nolte, R. J. M.

Self-Assembly of Disk-Shaped Molecules to Coiled-Coil Aggregates with Tunable Helicity. *Science* **1999**, *284*, 785−788. (c) Sommerdijk, N. A. J. M.; Holder, S. J.; Hiorns, R. C.; Jones, R. G.; Nolte, R. J. M. Self-Assembled Structures from an Amphiphilic Multiblock Copolymer Containing Rigid Semiconductor Segments. *Macromolecules* **2000**, *33*, 8289−8294.

(32) (a) Krappe, U.; Stadler, R.; Voigt-Martin, I. Chiral Assembly in Amorphous ABC Triblock Copolymers. Formation of a Helical Morphology in Polystyrene-block-polybutadiene-block-poly(methyl methacrylate) Block Copolymers. *Macromolecules* **1995**, *28*, 4558−4561. (b) Stadler, R.; Auschra, C.; Beckmann, J.; Krappe, U.; Voigt-Martin, I.; Leibler, L. Morphology and Thermodynamics of Symmetric Poly(A-block-B-block-C) Triblock Copolymers. *Macromolecules* **1995**, *28*, 3080−3097.

(33) (a) Li, C. Y.; Cheng, S. Z. D.; Ge, J. J.; Bai, F.; Zhang, J. Z.; Mann, I. K.; Harris, F. W.; Chien, L.-C.; Yan, D.; He, T.; Lotz, B. Double Twist in Helical Polymer "Soft" Crystals. *Phys. Rev. Lett.* **1999**, *83*, 4558−4561. (b) Li, C. Y.; Cheng, S. Z. D.; Ge, J. J.; Bai, F.; Zhang, J. Z.; Mann, I. K.; Chien, L.-C.; Harris, F. W.; Lotz, B. Molecular Orientations in Flat-Elongated and Helical Lamellar Crystals of a Main-Chain Nonracemic Chiral Polyester. *J. Am. Chem. Soc.* **2000**, *122*, 72−79.

(34) Nelson, J. C.; Saven, J. G.; Moore, J. S.; Wolynes, P. G. Solvophobically Driven Folding of Nonbiological Oligomers. *Science* **1997**, *277*, 1793−1796.

(35) Jung, J. H.; Kobayashi, H.; Masuda, M.; Shimizu, T.; Shinkai, S. Helical Ribbon Aggregate Composed of a Crown-Appended Cholesterol Derivative Which Acts as an Amphiphilic Gelator of Organic Solvents and as a Template for Chiral Silica Transcription. *J. Am. Chem. Soc.* **2001**, *123*, 8785−8789.

(36) Sone, E. D.; Zubarev, E. R.; Stupp, S. I. Semiconductor Nanohelices Templated by Supramolecular Ribbons. *Angew. Chem., Int. Ed.* **2002**, *41*, 1705−1709.

(37) Jamshidi, K.; Hyon, S. H.; Ikada, Y. Thermal Characterization of Polylactides. *Polymer* **1988**, *29*, 2229−2234.

(38) Fischer, E. W.; Sterzel, H. J.; Wegner, G. Investigation of the Structure of Solution Grown Crystals of Lactide Copolymers by Means of Chemical Reactions. *Colloid Polym. Sci.* **1973**, *251*, 980−1990.

(39) Miyata, T.; Masuko, T. Morphology of Poly(l-lactide) Solution-Grown Crystals. *Polymer* **1997**, *38*, 4003−4009.

(40) Kazmaier, P. M.; Hoffmann, R. A Theoretical Study of Crystallochromy. Quantum Interference Effects in the Spectra of Perylene Pigments. *J. Am. Chem. Soc.* **1994**, *116*, 9684−9691.

(41) Giaimo, J. M.; Lockard, J. V.; Sinks, L. E.; Scott, A. M.; Wilson, T. M.; Wasielewski, M. R. Excited Singlet States of Covalently Bound, Cofacial Dimers and Trimers of Perylene-3,4:9,10-bis(dicarboximide)s. *J. Phys. Chem. A* **2008**, *112*, 2322−2330.

(42) Wang, W.; Li, L.-S.; Helms, G.; Zhou, H.-H.; Li, A. D. Q. To Fold or to Assemble? *J. Am. Chem. Soc.* **2003**, *125*, 1120−1121.

(43) Balakrishnan, K.; Datar, A.; Oitker, R.; Chen, H.; Zuo, J.; Zang, L. Nanobelt Self-Assembly from an Organic n-Type Semiconductor: Propoxyethyl-PTCDI. *J. Am. Chem. Soc.* **2005**, *127*, 10496−10497.

(44) Xue, L.; Wu, H.; Shi, Y.; Liu, H.; Chen, Y.; Li, X. Supramolecular Organogels Based on Perylenetetracarboxylic Diimide Dimer or Hexamer. *Soft Matter* **2011**, *7*, 6213−6221.

(45) Zhao, C.; Zhang, Y.; Li, R.; Li, X.; Jiang, J. Di(alkoxy)- and Di(alkylthio)-Substituted Perylene-3,4;9,10-tetracarboxy Diimides with Tunable Electrochemical and Photophysical Properties. *J. Org. Chem.* **2007**, *72*, 2402−2410.

(46) Che, Y.; Datar, A.; Balakrishnan, K.; Zang, L. Ultralong Nanobelts Self-Assembled from an Asymmetric Perylene Tetracarboxylic Diimide. *J. Am. Chem. Soc.* **2007**, *129*, 7234−7235.

(47) Balakrishnan, K.; Datar, A.; Naddo, T.; Huang, J.; Oitker, R.; Yen, M.; Zhao, J.; Zang, L. Effect of Side-Chain Substituents on Self-Assembly of Perylene Diimide Molecules: Morphology Control. *J. Am. Chem. Soc.* **2006**, *128*, 7390−7398.

(48) Wang, Y.; Chen, H.; Wu, H.; Li, X.; Weng, Y. Fluorescence Quenching in a Perylenetetracarboxylic Diimide Trimer. *J. Am. Chem. Soc.* **2009**, *131*, 30−31.

(49) Wang, Q.; Chen, Y.; Ma, P.; Lu, J.; Zhang, X.; Jiang, J. Morphology and Chirality Controlled Self-Assembled Nanostructures of Porphyrin−Pentapeptide Conjugate: Effect of the Peptide Secondary Conformation. *J. Mater. Chem.* **2011**, *21*, 8057−8065.

(50) (a) Martin Wolffs, M.; George, S. J.; Tomović, Z.; Meskers, S. C. J.; Schenning, A. P. H. J.; Meijer, E. W. Macroscopic Origin of Circular Dichroism Effects by Alignment of Self-Assembled Fibers in Solution. *Angew. Chem., Int. Ed.* **2007**, *46*, 8203−8205. (b) Tsuda, A.; Alam, M. A.; Harada, T.; Yamaguchi, T.; Ishii, N.; Aida, T. Spectroscopic Visualization of Vortex Flows Using Dye-Containing Nanofibers. *Angew. Chem., Int. Ed.* **2007**, *46*, 8198−8202.

(51) Jonkheijm, P.; Hoeben, F. J. M.; Kleppinger, R.; Herrikhuyzen, J. V.; Schenning, A. P. H. J.; Meijer, E. W. Transfer of $\sigma$-Conjugated Columnar Stacks from Solution to Surfaces. *J. Am. Chem. Soc.* **2003**, *125*, 15941−15949.

(52) Chen, Z.; Stepanenko, V.; Dehm, V.; Prins, P.; Siebbeles, L. D. A.; Seibt, J.; Marquetand, P.; Engel, V.; Würthner, F. Photoluminescence and Conductivity of Self-Assembled $\pi-\pi$ Stacks of Perylene Bisimide Dyes. *Chem.-Eur. J.* **2007**, *13*, 436−449.

(53) Turner, J. F.; Riga, A.; O'Connor, A.; Zhang, J.; Collis, J. Characterization of Drawn and Undrawn Poly-L-lactide Films by Differential Scanning Calorimetry. *J. Therm. Anal. Calorim.* **2004**, *75*, 257−268.

(54) Yoshito, I.; Jamshidi, K.; Tsuji, H.; Hyon, S. H. Stereocomplex Formation between Enantiomeric Poly(lactides). *Macromolecules* **1987**, *20*, 904−906.

(55) Kowalski, A.; Duda, A.; Penczek, S. Kinetics and Mechanism of Cyclic Esters Polymerization Initiated with Tin(II) Octoate. (1) Polymerization of $\epsilon$-Caprolactone. *Macromol. Rapid Commun.* **1998**, *19*, 567−572.

(56) Boom, T.; Hayes, R. T.; Zhao, Y.; Bushard, P. J.; Weiss, E. A.; Wasielewski., M. R. Charge Transport in Photofunctional Nanoparticles Self-Assembled from Zinc 5,10,15,20-Tetrakis-(perylenediimide)porphyrin Building Blocks. *J. Am. Chem. Soc.* **2002**, *124*, 9582−9590.

(57) Percec, V.; Ahn, C. H.; Bera, T. K.; Ungar, G.; Yeardley, D. J. P. Coassembly of a Hexagonal Columnar Liquid Crystalline Superlattice from Polymer(s) Coated with a Three-Cylindrical Bundle Supramolecular Dendrimer. *Chem.-Eur. J.* **1999**, *5*, 1070−1083.

(58) Chen, H.; Xue, Q.; Li, Z.; Sun, L.; Zhang, Q. Synthesis and Characterization of Side Chain Polymer with Helical PLLA Segments Containing Mesogenic End Group. *Polymer* **2011**, *52*, 400−408.